Decay kinetics of nonequilibrium Al-Si solid solutions

N. E. Sluchanko, V. V. Glushkov, S. V. Demishev, and M. V. Kondrin*
General Physics Institute, Russian Academy of Sciences, Vavilov Str. 38, 117942 Moscow, Russia

T. V. Ischenko† and W. Gust
Institut für Metallkunde, Seestr. 92, D-70174 Stuttgart, Germany

V. V. Brazhkin
Institute of High Pressure Physics, Russian Academy of Sciences, 142092 Troitsk, Moscow District, Russia

B. B. Straumal
Institute of Solid State Physics, Russian Academy of Sciences, 142432 Chernogolovka, Moscow District, Russia

Y. Bruynseraede and V. V. Moshchalkov
Laboratory voor Vaste-Stoffysica en Magnetisme, Katholieke Universiteit Leuven, Celestijnenlaan 200, B-3001 Leuven, Belgium
(Received 16 April 1999; revised manuscript received 14 September 1999)

The decay kinetics and nonequilibrium state parameters of supersaturated substitutional solid solutions $Al_{1-x}Si_x$ ($x<20$ at. % Si) obtained by high-pressure synthesis have been studied comprehensively by resistivity relaxation and differential scanning calorimetry. It was shown that the decomposition process can be divided into two main stages. The first one consists of nucleation, growth, and coarsening processes usually observed during first-order phase transformations in metals and alloys. On the second stage the experimental data for isothermal relaxation and isochronal heat release can be explained assuming a nontraditional $\exp(-t/\tau)^{\alpha}$ kinetics with exponent $\alpha \approx \frac{1}{3}$. The drastic enhancement of the heat-release contribution at the latest stage of the phase separation is observed for $x \approx 6-8$ at. % Si. Further increase of Si concentration in the face-centered cubic (fcc) lattice of an Al-based solid solution leads to the formation of fcc Si clusters and initiates the splitting of the first stage of the decomposition process into three different branches. For any initial Si content, the second stage of the $Al_{1-x}Si_x$ phase transformation can be considered as a structural transition of fcc Si to tetrahedral Si inside of large Si clusters embedded in the Al-rich matrix.

I. INTRODUCTION

The kinetics of phase separation after quenching a binary alloy into the miscibility gap of the phase diagram is the problem of the great theoretical and practical interest.[1–3] The dominant processes observed are formation, growth, and coarsening of a second phase. One of the most convenient objects to study in this class of phenomena are nonequilibrium substitutional solid solutions formed from metal and semiconductor elements such as $Al_{1-x}Si_x$, where x is the mole fraction of the Si content. They can be obtained, for example, by a high-pressure treatment.[4]

The solubility of Si in Al drastically increases with increasing pressure:[4–5] the solubility limit is beyond 15 at. % Si at 5.4 GPa[4] in comparison with 1.5 at. % Si at atmospheric pressure.[6] The application of high pressures up to 10 GPa and rapid quenching to liquid-nitrogen temperature has allowed[6] to elevate the solubility limit up to 20 at. % Si (Fig. 1). An additional interest in Al-Si solid solutions is caused by a strong enhancement of the superconductivity in the vicinity of the lattice instability limit[7] [Fig. 2(a)]. The phase-separation process and the suppression of the superconductivity are closely related to each other in these materials. Moreover, an essential enhancement of the electron-phonon interactions has been found[7,8] in metastable Al-Si solid solutions, which can be attributed to the appearance of the so-called ''cluster phonon modes.'' Therefore, a comprehensive investigation of the nonequilibrium state of Al-Si solid solution appears as very attractive and will allow us to clarify both the features of the decay kinetics and the origin of the superconductivity enhancement in the vicinity of the instability of the face-centered cubic (fcc) lattice.

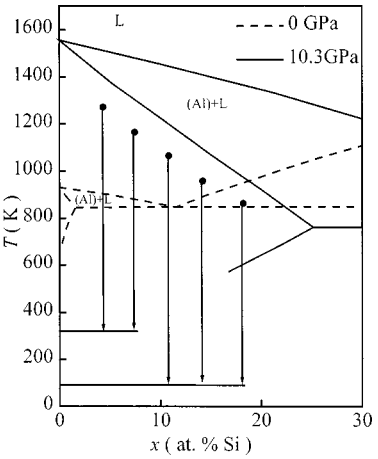

FIG. 1. Al-Si phase diagrams at normal pressure and 10.3 GPa. The arrows represent the synthesis scheme of the solid solutions formed under high pressure that are supersaturated at normal pressure. *L*, liquid; (Al), rich solid solution.

The available experimental data about the decay kinetics and heat-release effects of Al-Si solid solutions are incomplete and rather controversial. Recently published results on calorimetric measurements[9–11] are scarce, contradictory, and show essential variations of the heat release and activation parameters. Moreover, substantially supersaturated Al-Si solid solutions with Si contents between 10 and 20 at. % have not been studied yet.

In this work we have investigated in detail the decomposition process in fcc supersaturated solid solutions $Al_{1-x}Si_x$ followed by the formation of Si precipitates in the Al-rich matrix. To shed a light on the features of the decay kinetics and the origin of metastable phase formation in this system, we have studied both the samples with $x<0.08$ (temperature of transition into the superconductive state $T_C<6$ K, quenching under high pressure down to room temperature) and $0.08<x<0.2$ ($T_C<11$ K, quenching under high pressure down to liquid-nitrogen temperature). High-precision calorimetric measurements have been supplemented by isothermal resistivity relaxation studies of Al-Si nonequilibrium solid solutions.

II. EXPERIMENT

The samples of nonequilibrium fcc solid solutions $Al_{1-x}Si_x$ ($x<0.18$) have been obtained by high-pressure (up to 10 GPa) treatment in a Toroid chamber.[12] Cylinders of 4-mm height and 3-mm diameter were prepared from Al-Si alloys with $x=0.028-0.18$ homogenized at high pressure in the one-phase area of the Al-rich solid solution (Fig. 1). The pressure-temperature treatment procedure has been applied to these alloys inserted into NaCl pressed containers to avoid any injurious effects. The experimental details of the synthesis procedure, sample characterization, and preparation methods have been published elsewhere.[13] For polycrystalline fcc solid solutions with $x<0.08$, x-ray-diffraction spectra have been analyzed to verify the fcc single-phase structure and to estimate the Si content dispersion in $Al_{1-x}Si_x$ samples. As compared with the Al-Si alloys produced by rapid quenching at ambient pressure[14–16] the substitutional solid solutions $Al_{1-x}Si_x$ are homogeneous polycrystalline materials. The high-pressure-treatment technique allows us to eliminate the formation of quenched-in excess vacancies or vacancy aggregates[14–16] during the synthesis procedure.

To extend the range of the Si content in the fcc Al-based matrix and to prepare substantially nonequilibrium $Al_{1-x}Si_x$ solid solutions, the technique of rapid quenching under high pressure was applied with cooling to liquid-nitrogen temperature.[6] Supersaturated alloys with $x\approx0.085$, 0.12, 0.15, and 0.18 have been synthesized by this method (see Fig. 1). As long as the temperature of the superconducting transition T_C is proportional to the Si content[6] in the supersaturated solid solution [Fig. 2(a)], low-temperature magnetic susceptibility $\chi(T)$ measurements have been carried out [Fig. 2(b)] to determine the value of T_C and, therefore, to control the concentration of Si in the supersaturated solid solution. The $\chi(T)$ data obtained for alloys with $x\leqslant0.08$ are very similar to the results reported previously.[13] In the case of nitrogen-cooled samples with $x>0.08$, the concentration of Si in the Al-based matrix was tested without any destructive overheat by loading the magnetometer at liquid-nitrogen

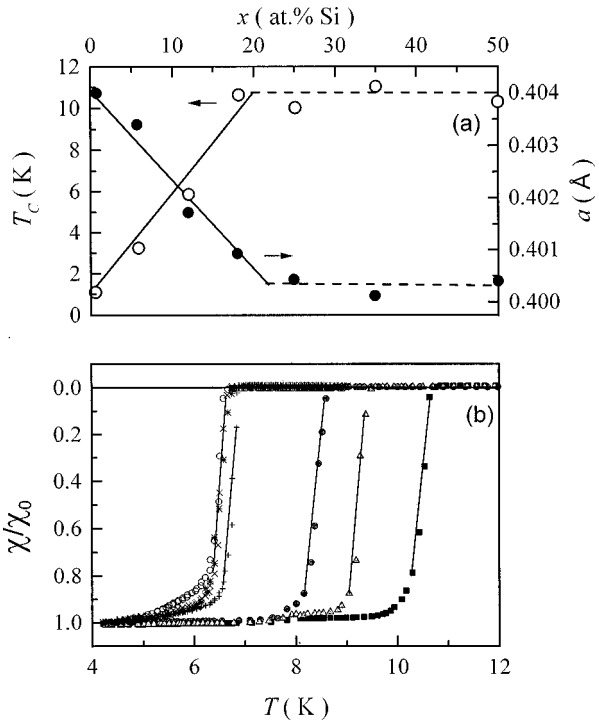

FIG. 2. (a) Dependence of the superconducting transition temperature T_C (open circles) and lattice constant (solid circles) of Al-Si solid solutions on the Si concentration (Ref. 5). (b) Normalized magnetic susceptibility χ/χ_0 of the investigated samples around the superconducting transition temperature.

temperature. Additionally, the investigation of two different $Al_{0.915}Si_{0.085}$ samples quenched under pressure to room temperature and liquid-nitrogen temperature has been performed to prove T_C in order to ensure that the Si content in the supersaturated solid solution is the same. When the samples were stored at temperatures below 270 K after the pressure-temperature treatment, no difference was found between these materials synthesized in different ways.

The decomposition kinetics has been studied by an isothermal resistivity relaxation method (Van der Pauw scheme of resistivity measurements with four terminals; see, for example, Ref. 17) and the differential-scanning calorimetry, (DSC) technique. To get DSC measurements of high precision a homemade installation has been applied (Fig. 3). The sample (1) was loaded into the sample holder (2, miniature copper containers). The duplicate holder contains a standard pure-Al cylinder (3) of a mass of 90 mg. The containers with samples were glued to the thin cotton threads (4) inside the copper radiation shield (5). The sample holder's assembly was located in the exchange helium gas (pressure about 20 kPa) and enclosed in a jacket (6) inside the liquid-nitrogen Dewar container. Copper-constantan thermocouples (7–9) were used for the measurement of the temperature T and temperature gradients ΔT. The isochronal heating rates were varied in the interval 0.5–10 K/min. A special small heater (10) was used in addition to the oven (11) to calibrate the absolute heat-release effects. The simultaneous application of precision-temperature controller and Keithley 2182 dual-channel nanovoltmeter allowed us to reach a sensitivity better than 20 nV or 0.0005 K for the temperatures under investigation.

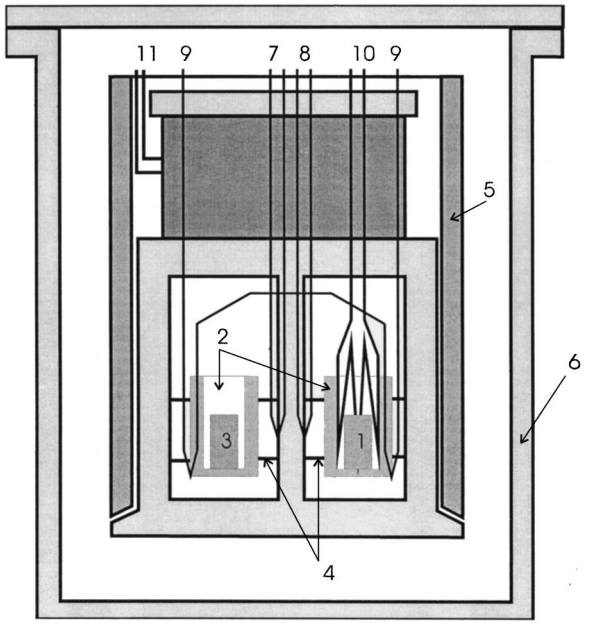

FIG. 3. The cryogenic assembly used for the DSC measurements (see text).

As long as the metastable state of $Al_{1-x}Si_x$ solid solutions is found to be sensitive to the electron-beam exposure, we were limited in the application of electron-microscopy technique to the samples structure characterization. Therefore only the final state of the decomposition process of $Al_{1-x}Si_x$ solid solutions was investigated by transmission electron microscopy[18] and by light microscopy with the aid of a NEOPHOT optical microscope.

III. RESULTS

A. Resistivity measurement

To establish the kinetics of solid-state transformation of the supersaturated $Al_{1-x}Si_x$ solid solutions, the time dependence of isothermal resistivity has been investigated for samples with $x \approx 0.035$ (Fig. 4) and $x \approx 0.075$ (Fig. 5). In accordance with Ref. 17, the residual resistivity changes $\rho_0(x)$ can be used to evaluate the transformed volume fraction during the decomposition process in $Al_{1-x}Si_x$. Moreover, the so-called metastable contribution $\Delta\rho \sim \rho_0$ in the resistivity of these alloys depends on the Si concentration in the fcc Al-rich matrix.[17] Therefore, it is possible to analyze the features of the decomposition process through the study of the resistivity relaxation behavior $\Delta\rho(T,t)$ (Figs. 4 and 5). $\Delta\rho$ is determined as the difference between the actual resistivity ρ and the ''final'' resistivity ρ_∞, corresponding to a very long annealing time t. For the quantitative analysis of the resistivity data it is very important to determine the ''final'' resistivity curves $\rho_\infty(t,T) = \lim_{l\to\infty} \rho(t,T)$. The $\rho_\infty(T)$ dependence was obtained by temperature measurements of the samples completely annealed at $T = 620$ K and then $\rho_\infty(T)$ were used to extract the nonequilibrium contribution $\Delta\rho(t,T)$.

The decay kinetics studied by the isothermal resistivity measurements $\rho(t, T = \text{const})$ of the alloys demonstrates a complicated behavior during the phase-separation process.

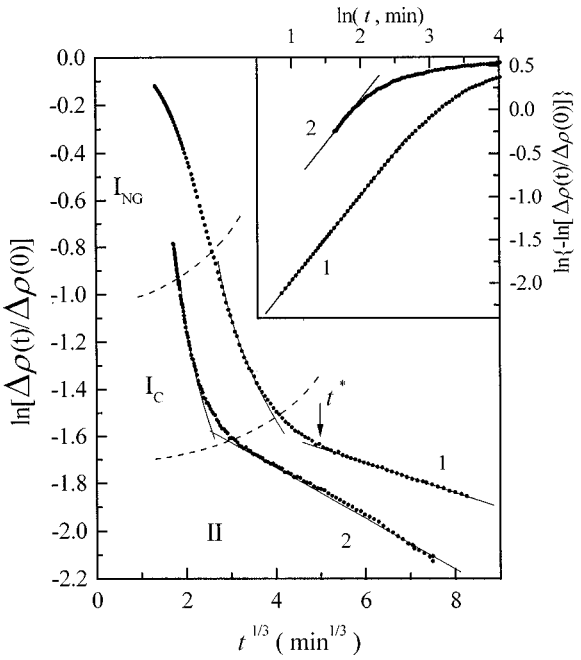

FIG. 4. Relaxation of the electrical resistivity of an $Al_{0.965}Si_{0.035}$ sample measured at 496 K (1) and 521 K (2). In the inset the initial sections of both curves are shown.

There are two well-defined stages on the resistivity relaxation curves (Figs. 4 and 5, I and II) that can be attributed to a ''fast'' and ''slow'' relaxation process during the decomposition of these nonequilibrium solid solutions.

The first one causes the largest change in $\Delta\rho(t) = \rho(t) - \rho_\infty$. Following the approach based on the Avrami equation, one can write for the transformation rate ζ (ζ being the ratio of transformed volume to the whole volume of the sample)

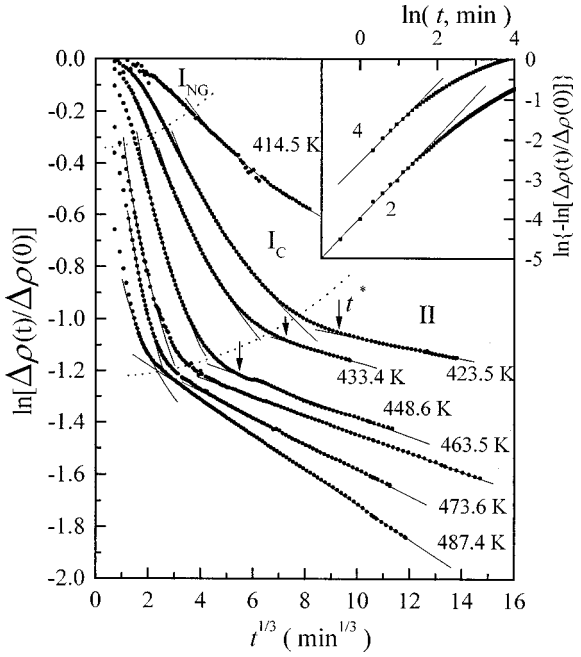

FIG. 5. Relaxation of the electrical resistivity of an $Al_{0.925}Si_{0.075}$ sample measured at several temperatures. In the inset the initial sections of two curves are shown.

$$\zeta = 1 - \exp[-(t/\tau)^n], \quad (1)$$

where n is the Avrami constant depending on the nucleation and growth mechanisms and τ is the characteristic time. Assuming $\zeta \sim \Delta\rho$, the initial stage (part I of the resistivity relaxation curves in Figs. 4 and 5) can be identified as an exponential relaxation to the equilibrium state ($n = 1 \pm 0.1$, see also the inset in Fig. 4). This agrees with the well-known results for various supersaturated metallic alloys.[19] As it was established in our previous investigations,[17,20] the nucleation and growth process (I_{NG}, Figs. 4 and 5) is followed by the coarsening (I_C, Figs. 4 and 5).

According to previously published results,[20] one can consider the change of the coarsening exponent

$$\zeta \sim t^{-\alpha} \quad (2)$$

in Al-Si solid solutions as a result of the transition from a coarsening-type behavior ($\alpha \approx 0.16$) at relatively low annealing temperatures to an evaporation-condensation process (Lifshitz-Sleozov kinetics, $\alpha = 0.33$) for $T \geqslant 450$ K (see also Fig. 2 in Ref. 20). However, the power law (2) with $\alpha = 0.16-0.33$ holds only up to $t < t^*$ (see Figs. 4 and 5). For $t > t^*$ the kinetics changes dramatically and in this region the experimental curves can be approximated better by a very unusual exponential behavior (1) with $n \approx 0.33$ (see part II of the resistivity relaxation curves in Figs. 4 and 5). It is worth noting here that the exponent $\zeta \sim \exp(-At^{1/3})$ provides us the best approximation for the widest range of Si concentrations ($x < 0.2$) and for the annealing temperatures investigated. Moreover, Eq. (1) with $n \approx 0.33$ provides a better approximation for the experimental data of nonequilibrium solid solutions quoted in Figs. 4 and 5 than any kind of analytical dependence for a coarsening process such as the Liftshitz-Sleozov expression $\zeta \sim t^{1/3}$ or other scaling exponents ($t^{-1/5}, t^{-1/6}$) (see Refs. 1–3). It is worth noting that in our previous work[20] the experimental data for the resistivity at $t > t^*$ were fitted by Eq. (2) with $\alpha \approx 0.08-0.09$ on the latest stage of the decomposition process. It was discussed in terms of the cluster growth kinetics in Al-Si solid solutions.[20] However, the approximation $\zeta \sim t^{-0.08}$ used in Ref. 20 failed to describe the experimental results for high annealing temperatures and long annealing times, where Eq. (1) with $n = 0.33$ works well (Figs. 4 and 5).

B. DSC data for $x \leqslant 0.08$

The resistivity data may be sensitive to the distribution of Si clusters formed during the decomposition of the metastable solid solution and are effected by the global topology of the nonhomogeneous system (so-called percolation effects). Sometimes the distribution of Si clusters may effect the results of the resistivity measurement. Therefore, we applied also the DSC technique to establish the mechanisms of phase separation. The DSC measurements were made for the same samples of supersaturated solid solutions (cut from the Al-Si cylinders obtained at the high pressure) with $x \approx 0.03-0.04$ [Fig. 6(a)] and $x \approx 0.075$ [Fig. 6(b)]. Therefore, the measurements have been carried out in the interval of Si contents intensively studied in Refs. 9–11.

For samples with $x \approx 0.03-0.04$ [Fig. 6(a)] the heat-release effect has a single peak in the range of isochronal annealing rates applied (0.5–10 K/min). For Si contents between 6 and 9 at. %, a double peak structure of the DSC spectra has been found [Fig. 6(b)]. It is worth mentioning that the two well-distinguished stages I and II of the decomposition process during isothermal annealing (Figs. 4 and 5) correspond only to one feature in our heat-release results for supersaturated Al-rich alloys with $x \leqslant 0.06$ Si at annealing temperatures below 550 K. At the same time, for Si contents in the interval $0.06 < x < 0.09$, the relaxation processes I and II are well identified in the isothermal and isochronal annealing measurements. It is necessary to note that such a kind of DSC behavior agrees qualitatively with previous results.[9–11]

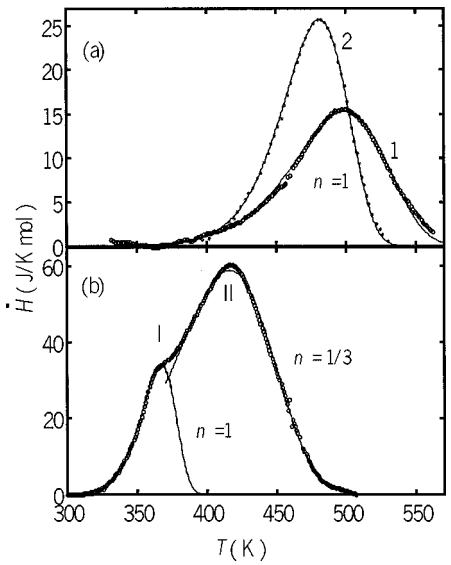

FIG. 6. DSC curves as measured with an isochronal annealing rate of (a) 2 K/min on an $Al_{0.915}Si_{0.085}$ sample (solid circles) and (b) 10 K/min on the samples $Al_{0.965}Si_{0.035}$ (1) and $Al_{0.96}Si_{0.04}$ (2) from Ref. 11. The lines show the fit calculated with the Avrami formula.

To determine the Si nonequilibrium state parameters of Al-Si solid solutions the DSC experiments with different annealing rates have been performed. The typical family of

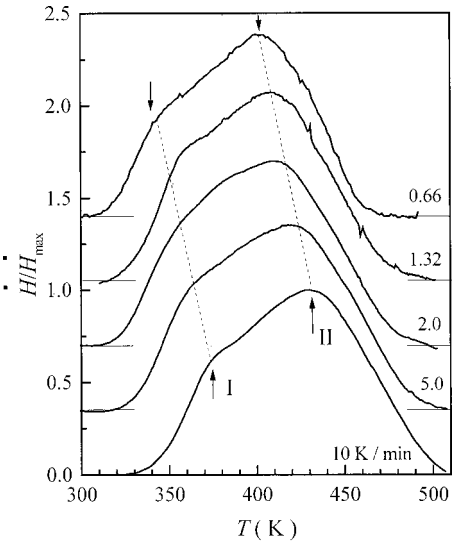

FIG. 7. Normalized heat release of the $Al_{0.915}Si_{0.085}$ samples measured with different rates. The arrows and lines show the shift of the peak positions.

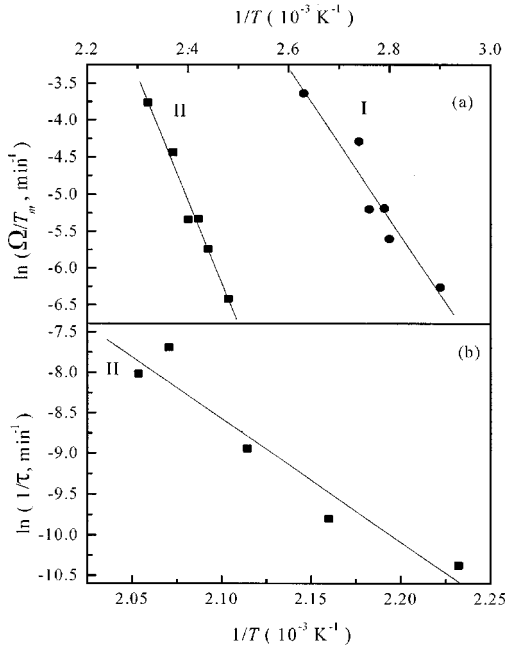

FIG. 8. Arrhenius plots for $Al_{0.915}Si_{0.085}$. (a) Evaluation of the activation parameters for the processes I (circles) and II (squares) based on the differential-thermal-analysis data (Fig. 7). The lines are guides for the eye. (b) The characteristic time τ for process II is evaluated from resistivity relaxation data (Fig. 5).

normalized $dH/dT=f(T)$ curves are presented in Fig. 7. In the framework of the traditional approach, the data shown in Fig. 7 ($x\approx 0.085$) and similar results for samples in the concentration range $x\leqslant 0.06$ were used to evaluate both the activation energy E_a and the preexponential factor τ_0^{-1} (the atomic displacement frequency).

The temperature dependence of the ratio Ω/T_m (where Ω is the heating rate and T_m is the temperature of the maximal heat release) for $Al_{0.915}Si_{0.085}$ ($T_C\approx 6.5$ K) in the Arrhenius coordinates $\ln(\Omega/T_m)=f(1/T_m)$ is shown in Fig. 8(a). In Fig. 8(b) the Arrhenius dependence of the resistivity relaxation parameter $1/\tau$ for the sample with $x\approx 0.075$ is shown. As determined in Fig. 8, the values of the activation energy and the pre-exponential factor [$E_{aI}=85$ kJ/mol, $\tau_{0I}^{-1}=2.0\times 10^8\ s^{-1}$; $E_{aII}=139$ kJ/mol, $\tau_{oII}{}^{-1}=2.8\times 10^{13}\ s^{-1}$, Fig. 8(a), and $E_{aII}=149$ kJ/mol, $\tau_{0II}{}^{-1}=2.0\times 10^{12}\ s^{-1}$, Fig. 8(b)] are in good agreement with the results of ''step-by-step'' annealing resistivity relaxation experiments.[17] Unfortunately, the precision of the previous DSC measurements of Al-Si nonequilibrium solid solutions[9–11] was not high enough to extract direct information about the behavior of the pre-exponential factor $\tau_0{}^{-1}$. Therefore, the $\tau_0{}^{-1}$ values (Fig. 8) can be compared only with isothermal relaxation results.[17]

Another way to verify the activation parameters E_a and $\tau_0{}^{-1}$ deduced from the DSC experiments (Figs. 6 and 7) is to apply directly the equations of thermal analysis for approximation of heat-release effects. Indeed, the isochronal annealing ($\Omega=$ const) expression

$$-\ln(1-\zeta)=\left[\int_{T_\phi}^{T}\frac{1}{\Omega\tau_0}\exp\left(-\frac{E_a}{T'}\right)dT'-\ln^{1/n}(1-\zeta_0)\right]^n. \tag{3}$$

can be used to evaluate the Avrami constant n together with E_a and $\tau_0{}^{-1}$ (Fig. 8) in developing of a $dH/dT=f(T)$ fitting procedure. It was quite usual to apply for this purpose the numerical approximation based on the E_a and $\tau_0{}^{-1}$ parameters as determined from the DSC data for various heating rates (Fig. 7). After that, the fitting of calorimetric results given in Figs. 6 and 7 can be carried out in the framework of expression (3) or relative integro-differential equation,

$$\begin{aligned}\frac{d\zeta}{dt}&=\Omega(1-\zeta)\frac{d}{dT}\left[\int_{T_\phi}^{T}\frac{1}{\Omega\tau_0}\exp\left(-\frac{E_a}{T'}\right)dT'-\ln^{1/n}(1-\zeta_0)\right]^n\\&=\Omega\frac{d}{dT}\left[\int_{T_\phi}^{T}\frac{1}{\Omega\tau_0}\exp\left(-\frac{E_a}{T'}\right)dT'-\ln^{1/n}(1-\zeta_0)\right]^n\\&\quad\times\exp\left\{-\left[\int_{T_\phi}^{T}\frac{1}{\Omega\tau_0}\exp\left(-\frac{E_a}{T'}\right)dT'-\ln^{1/n}(1-\zeta_0)\right]^n\right\},\end{aligned} \tag{4}$$

and n value is varied to obtain the best approximation for the DSC results shown in Figs. 6 and 7 with E_a and $\tau_0{}^{-1}$ parameters compared with the aforementioned values (Fig. 8). Finally, Eq. (4) was applied for the fitting of calorimetric data in the following presentation:

$$\begin{aligned}\frac{dH}{dT}&=B\left[\int_{T_\phi}^{T}\exp\left(-\frac{E_a}{T'}-\ln(\Omega\tau_o)\right)dT'-\ln^{1/n}(1-\zeta_o)\right]^{n-1}\exp\left[-\frac{E_a}{T}-\ln(\Omega\tau_o)\right]\\&\quad\times\exp\left\{-\left[\int_{T_\phi}^{T}\exp\left(-\frac{E_a}{T'}-\ln(\Omega\tau_o)\right)dT'-\ln^{1/n}(1-\zeta_o)\right]^n\right\}.\end{aligned} \tag{5}$$

The parameter ζ_o was determined directly from the normalized DSC spectra and additionally the least-squares method was applied for the calculation of the parameter B.

The results of the approximation in the framework of the aforementioned approach Eqs. (3)–(5) are shown in Figs. 6(a) and 6(b). For DSC spectra with double peak structure [Fig. 6(b)] the additivity of the contributions of the processes I and II to the total heat-release effect was not supposed and the left and right ''slopes'' of the $dH/dT=f(T)$ curves have been fitted as fast (I) and slow (II) relaxation inputs, respectively.

One of the most interesting results, which can be deduced from the suggested analysis (3) to (5) of the DSC spectra shown in Figs. 6 and 7, is the quantitative agreement between the experimentally determined Avrami exponents (Figs. 4 and 5) and the calculated values $n_1=1\pm 0.1$ and $n_{II}=0.34\pm 0.04$. Moreover, the activation parameters detected from the self-consistent approach are very close to the values $E_{aI}=80\pm 10$ kJ/mol, $E_{aII}=135\pm 15$ kJ/mol, $\tau_{oI}{}^{-1}=10^6-10^9\ s^{-1}$, and $\tau_{oII}{}^{-1}=10^{10}-10^{13}\ s^{-1}$ in the Si concentration range $x\leqslant 0.08$.

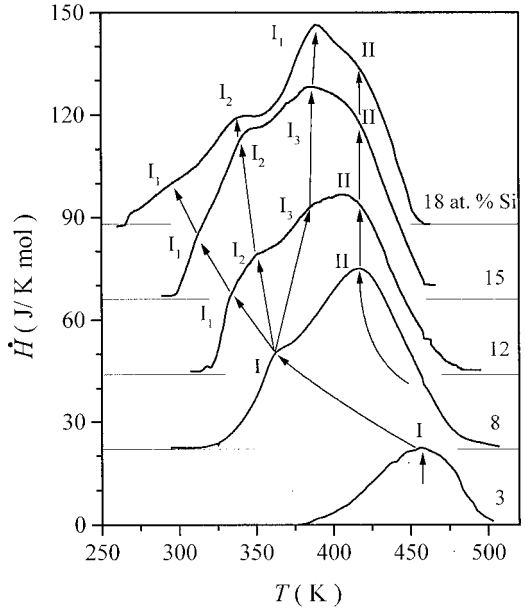

FIG. 9. DSC spectra of several Al-Si alloys as measured with an isochronal annealing rate of 2 K/min. The arrows show the shift of the peaks.

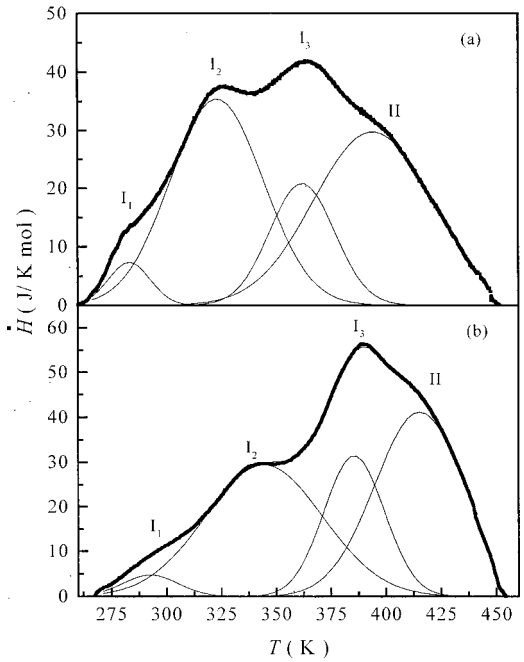

FIG. 10. DSC curves of $Al_{0.82}Si_{0.18}$ samples measured with different rates: (a) 0.66 K/min and (b) 2 K/min. In both cases the thin lines show the multi-Gauss fit of the curves.

C. DSC data for Si content $x>0.08$

The double peak structure of the DSC spectra for $x \approx 0.06-0.08$ [Fig. 6(b)] changes dramatically for supersaturated solid solutions with a Si content $x \geqslant 0.085$. The DSC spectra are shown in Fig. 9 for substantially supersaturated Al-Si alloys in comparison with the $dH/dT=f(T)$ results for $Al_{0.965}Si_{0.035}$. It is necessary to note that there is a more complicated character of the heat-release effect for samples with $x>0.09$. There are four different inputs in the DSC curves that can be easily distinguished by different isochronous rate experiments in this Si concentration range. The input II (highest temperature) is presented on the DSC spectra in the wide range $x \geqslant 6$ at. % Si and is connected with an Avrami-type ($n \approx 0.33$) phase-separation process. The appearance of three different contributions (I_1,I_2,I_3) in the $dH/dT=f(T)$ dependence for $x \geqslant 0.09$ can be considered as a ''splitting'' of the fast relaxation DSC maximum (I) when the Si content increases (Fig. 9). Moreover, the experiment with different rates of isochronous annealing allows us to separate quantitatively different contributions (I_1,I_2,I_3) for samples with the highest Si content ($x \approx 0.18$, $T_C \approx 10.5$ K, see Fig. 10). The separation of four different inputs was performed here by application of Gauss-type functions (I_1,I_2,I_3,II) for the description of the total heat-release effect. The I_1, I_2, I_3, and II contributions in the total DSC spectra are not necessarily additive. If we suppose that they are additive, it allows us to find out and to analyze separately the heat-release inputs [Fig. 11(b)] and the activation parameters (Fig. 12) for the I_1, I_2, I_3, and II processes.

It is worth mentioning that the numerical thermal analysis (3) to (5) has also been applied here to estimate the parameters n, E_a, and τ_o^{-1} directly from the DSC spectra shown in Figs. 9 and 10. The left and right slopes of the total $dH/dT=f(T)$ curves (see Figs. 9 and 10) were analyzed with Eqs. (3)–(5), and the values of n, E_a, and τ_o^{-1} were deduced for the process II ($n \approx 0.33$, $E_{a\mathrm{II}}=130\pm12$ kJ/mol, $\tau_{o\mathrm{II}}{}^{-1}=10^{12}-10^{14}\,\mathrm{s}^{-1}$) and sometimes (where it was possible) for the I_1, I_2, and I_3 stages of the phase transformation. The results of these estimations are presented in Fig. 12 together with previously published data.[17,20]

Finally, it is quite clear from the results shown in Figs. 9 and 10 that at room temperature the supersaturated solid solutions with $x>0.09$ are substantially nonequilibrium. Indeed, the first stage of phase transformation (process I_1, Figs. 9 and 10) occurs fast enough around $T \approx 270-300$ K, so the rapid quenching to liquid-nitrogen temperature under high pressure and storing at intermediate temperatures are needed to avoid the decomposition of these model superconductors.

IV. DISCUSSION

According to the experimental data shown in Figs. 4–10, the variation of the nonequilibrium state parameters and the decay kinetics allows us to consider three intervals ①, ②, and ③ on the scale of the Si concentration (① corresponds to $x<0.06$, ② to $0.06<x<0.09$, and ③ to $x>0.09$).

A. $Al_{1-x}Si_x$ with $x<0.06$ and $0.06 \leqslant x<0.09$ (intervals ①–②)

From the point of view of the decay kinetics (Figs. 4 and 5), there is no difference between the ① and ② intervals of the Si content in $Al_{1-x}Si_x$. Indeed, the main process I of nucleation, growth, and coarsening can be deduced as a fast one dominating in the change of the amplitude of $\Delta\rho(T,t)$ (Figs. 4 and 5). The latest stage of the decomposition process (II) produces relatively slow changes in the metastable part of the resistivity. Therefore, it is quite possible to understand why in our measurements shown in Fig. 6(b) we could not register the heat-release effects from this process (II) for Si concentrations $x<0.06$ and annealing temperatures below 550 K.

There are several effects, which can be expected when the concentration of Si increases in a fcc Al-based matrix. The

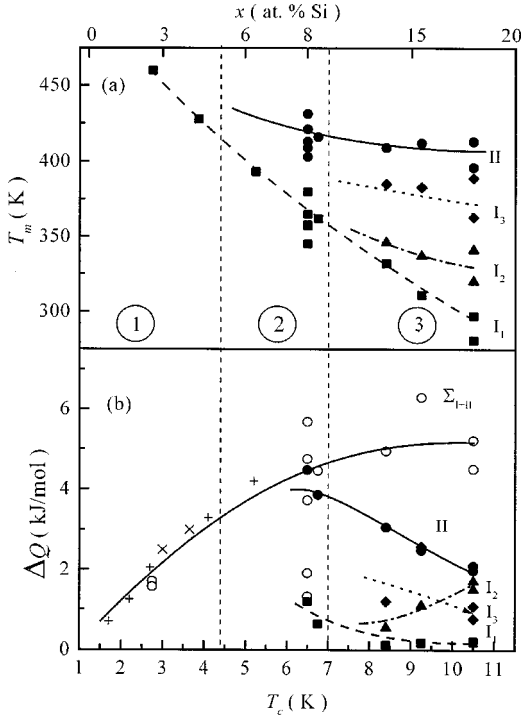

FIG. 11. (a) Peak position and (b) heat release of the elementary processes versus superconducting transition temperature T_C (or Si content). The lines are guides for the eyes. Curve Σ_{I+II} corresponds to the total heat release. The values + and × are drawn from Refs. 11 and 12, respectively.

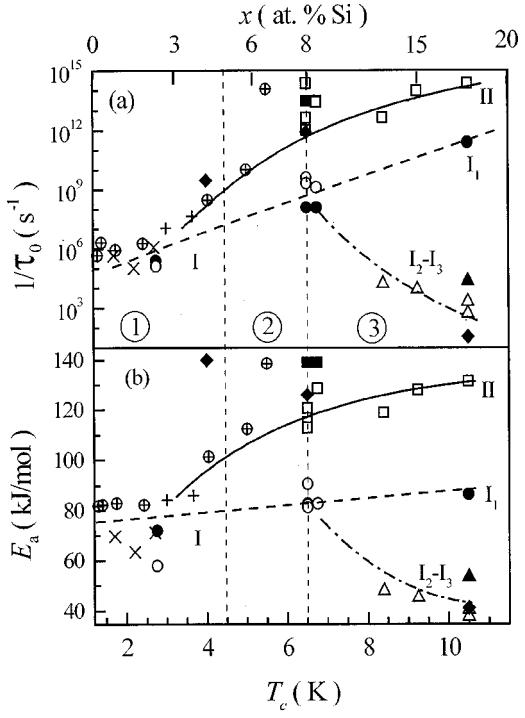

FIG. 12. Activation parameters E_a and τ_0^{-1} of the elementary processes versus the superconducting transition temperature T_C and Si content. The solid symbols correspond to values as determined from different isochronal rate experiments, the open symbols are the values calculated by the numerical procedure due to Eqs. (3)–(5). The lines are guides for the eyes. The values +, ×, and ⊕ are obtained from the thermal analysis [Eqs. (3)–(5)] of the data from Refs. 10, 11, and 20, respectively.

exothermal effect is associated with the nonequilibrium (metallic) state of the Si atoms included in the fcc lattice of the solid solution.[6–9] Therefore, the linear enlargement of enthalpy ΔQ [Fig. 11(b)] can be attributed to additive individual contributions from the distortion of the fcc lattice around the included Si atoms in the concentration range ①. Another remarkable feature is the substantial shift of the whole $dH/dT=f(T)$ peak towards lower temperatures as the Si concentration increases [Fig. 11(a)]. It is worth mentioning that the temperature of the maximal heat release $T_m(x)$ changes rapidly in the interval ① (about 15 K/at. % Si). This value is comparable with the results of Ref. 11 where from DSC data the magnitude $dT_m/dx \approx 10-12$ K/at. % Si can be deduced. The difference between these two rates can be caused by the initial presence of semiconducting Si precipitates in the Al-Si samples studied in Ref. 11. Indeed, the superconducting transition temperature value $T_C<4$ K for $Al_{0.92}Si_{0.08}$ reported in Ref. 11 is essentially smaller than the real magnitude $T_C(Al_{0.92}Si_{0.08})=5.5-6$ K (Fig. 11). Besides, due to the proportionality of T_C to x [see Fig. 2(a)], a certain discrepancy can appear in a quantitative comparison of our calorimetric results (Figs. 6–12) with the DSC data.[9–11] To avoid this disagreement one needs evidently to correct the Si contents reported in Refs. 9–11 to smaller values of x.

It is also interesting to note that the additional features of the heat-release effect of Al-Si alloys have been found in the temperature range $T>540$ K.[11] In this temperature interval the measurements cannot be made by our DSC experimental setup. For these annealing temperatures one can expect an appearance of the heat-release contribution from the latest stage process (slow process II). Therefore, these DSC peculiarities, which were not discussed previously,[11] could be considered as the ''imprint'' of the section II of the phase transformation. For low-Si concentrations ($x<0.06$, interval ①) the stage-II process contribution in the heat release is much smaller in comparison with the main part enthalpy changes (fast process I). Moreover, the activation parameters $E_{aII} \approx 130 \pm 10$ kJ/mol, $\tau_{oII}^{-1} \approx 10^9-10^{13}$ s^{-1} of stage II (precipitates formation) is very closely related to the activation energy of Si diffusion in the pure-Al matrix [$E_a^{Al}(Si) \approx 128$ kJ/mol]. At the same time, the remarkable variation of the preexponential factor τ_{oII}^{-1} can be established from the resistivity relaxation measurements shown in Figs. 4 and 5. The τ_{oII}^{-1} parameter changes between 2×10^9 s^{-1} for $x \approx 0.035-0.04$ and $10^{13}-10^{14}$ s^{-1} for $x \approx 0.075-0.08$. Therefore, the increase of the Si content is accompanied not only by an enhancement of the exothermal effect of process II but also by an acceleration of the decay kinetics at this stage of the phase transformation.

Section II of the decomposition process is followed to an evaporation-condensation process of Si submicrometer inclusions in the Al-rich matrix (Lifshitz-Sleozov kinetics, stage I_C in Figs. 4 and 5) and, hence, it could be considered as a so-called ''generalized coarsening'' stage of the phase transformation. On the other hand, the kinetics of the processes I and II has a dramatic crossover and there is a very large exothermal effect during the stage II. It allows one to suppose that the phase transition from fcc Si to tetrahedral Si (from a 12- to a 4-coordinated lattice) takes place inside of

large enough Si clusters embedded into the Al-rich matrix. From this point of view, one can expect a very large heat-release effect during the short-range order reconstruction as well as a strong dependence of the size and concentration of the Si clusters on the rate of process II.

The problem discussed is closely related to the problem of a crystalline structure of small Si clusters[21,22] (10–100 atoms) and involved recently in active discussion.[23–25] Indeed, in Refs. 21 and 22 the total energy of fragments with diamond and fcc structure was calculated as a function of the number of atoms they contain. It was shown[20,21] that the metallic structure is favored over the covalent one for clusters containing less than about 50 atoms. Evidently, the situation is much more complicated for nonequilibrium Al-Si solid solutions where large Si clusters are surrounded by a strongly distorted Al-based fcc matrix, that changes noticeably the interphase boundary energy of the Si clusters.

Following the present approach, one can consider the value of the activation energy of the second process ($E_{a\mathrm{II}} \approx E_a^{\mathrm{Al}}(\mathrm{Si}) \approx 130$ kJ/mol) as a result of diffusion-controlled growth of the large fcc Si clusters up to a critical size. Then the transition to a covalent-type bond occurs and the fcc Si clusters transform into tetrahedrally coordinated Si particles.

In the framework of the suggested interpretation one can roughly estimate the variation of the microscopic $l(x)$ and macroscopic $L(x)$ mean lengths of the Si atom diffusion during stage II in the concentration range from 3.5 at. % Si (Fig. 4) to 7.5 at. % of Si (Fig. 5). The comparison between the characteristic times l^* (onset of process II, see Fig. 4) of the crossover region as well as the preexponential factor $\tau_{o\mathrm{II}}$ allows one to evaluate the ratio $L(x \approx 0.035)/L(x \approx 0.075) \approx 3.5$ and $l(x \approx 0.035)/l(x \approx 0.075) \approx 10^2$ for these Al-Si alloys. One can see that the $L(x)$ parameter decreases essentially (by a factor of 3.5) when the Si concentration increases two times. It seems to be reasonable that the $L(x)$ ratio represents an estimation of the change of the mean distance between the Si precipitates in the Al-based matrix. The variation of the microscopic length $l(x)$ were deduced from $\tau_{o\mathrm{II}}$ $(x \approx 0.035) \approx 4.5 \times 10^{10}$ s and $\tau_{o\mathrm{II}}(x \approx 0.075) \approx 10^{-14}$ s (Figs. 4, 5, and 8) and is more pronounced (about a factor of 10^2). It corresponds probably to very complicated diffusion trajectories of the Si atoms during the latest decomposition stage of these nonequilibrium alloys.

The established violation of the Lifshitz-Sleozov regime is accompanied by essential changes both of the size distribution of the Si clusters and of the mean cluster radius. It is worth noting here the results of Blaschko *et al.*[26] obtained in experiments on the diffuse neutron scattering. A similar crossover of the $\zeta \sim t^{-1/3}$ behavior and the power law $\zeta \sim t^{-0.08}$ have been observed for various compositions of Al-Zn-Mg alloys.[26] A possible explanation of the crossover between stages I and II in the case of these alloys could be deduced again from the similar hypothesis that a phase transformation from the fcc to hcp Zn-Mg clusters proceeds inside large Zn-Mg clusters embedded in the Al-rich matrix.

An additional argument in favor of the present interpretation of the fcc to diamond structure phase transition in the large Si clusters embedded into the Al-based fcc matrix can be deduced from TEM and small-angle neutron-scattering experiments. In particular, TEM analysis has been carried out for inhomogeneous Al-Si alloys that are the final equilibrium (eutectic) state obtained by the decomposition of metastable $Al_{1-x}Si_x$ solid solutions. The results of the TEM study allow us to estimate the size d of the semiconducting Si regions in Al-rich matrix: $d \leqslant 100$ Å. It is worth mentioning also that a similar conclusion has been obtained in Ref. 27, where the small-angle neutron-scattering experiments have been done for different decay stages of the $Al_{1-x}Ge_x$ solid solutions. From the data of isochronal annealing it was established[27] that the size of the semiconducting regions increases slightly during the decomposition. The estimated d value happens to depend on both the annealing temperature and the initial Si content and changes in the range 30–60 Å.[27]

In the framework of the above-mentioned interpretation it is important also to re-examine the results of the ''step-by-step'' annealing resistivity relaxation experiments on Al-Si alloys.[17,20] The activation law parameters obtained from these experimental data[17,20] are closely related to the E_a and τ_o^{-1} values [see Figs. 12(a) and 12(b)] for supersaturated solid solutions in the interval ①. A further increase of the Si content drastically enhances the contribution of process II both in the heat release and in the resistivity relaxation characteristics. As a result one can observe the appearance of intermediate (mixed) values of E_a and τ_o^{-1} (80 kJ/mol $< E_a < 130$ kJ/mol and $10^7\ \mathrm{s}^{-1} < \tau_o^{-1} < 10^{13}\ \mathrm{s}^{-1}$) in the concentration range 6–8 at. % Si [Figs. 12(a) and 12(b)].

B. Substantially supersaturated $Al_{1-x}Si_x$ alloys ($x \geqslant 0.09$)

In comparison with the $E_{a\mathrm{II}}$ and $\tau_{o\mathrm{II}}^{-1}$ characteristics behavior in the range $x \approx 0.06$–0.08 there is no qualitative change during the stage II of the phase separation process (Figs. 11 and 12). Indeed, the $T_{m\mathrm{II}}(x)$, $E_{a\mathrm{II}}(x)$, and $\tau_{o\mathrm{II}}^{-1}(x)$ parameters are not changed noticeably in the wide interval 9–20 at. % Si (Figs. 11 and 12; interval ③). At the same time the heat-release contribution $\Delta Q_{\mathrm{II}}(x)$ of the process II is reduced essentially [Fig. 11(b)] together with the appearance and elevation of various releases $\Delta Q_{\mathrm{I}_1}(x)$, $\Delta Q_{\mathrm{I}_2}(x)$, and $\Delta Q_{\mathrm{I}_3}(x)$ of the exothermic channels corresponding to the stage-I process. Moreover, from the saturation of the total heat release $\Delta Q_{\Sigma=\mathrm{I}+\mathrm{II}}(x)$ one can conclude that the variations of $\Delta Q_{\mathrm{I}}(x)$ and $\Delta Q_{\mathrm{II}}(x)$ compensate each other within the interval 9–20 at. % Si.

On the contrary, the ''splitting'' of process I into three branches I_1–I_3 (Figs. 9–12) is observed for a Si content of 8.5–9 at. %. It is accompanied by drastic changes of the $E_{a\mathrm{I}}$ and $\tau_{o\mathrm{I}}^{-1}$ parameters. Among the I_1–I_3 sections of stage I, only the process I_1 demonstrates the same tendency of the $E_a(x)$ and $\tau_o^{-1}(x)$ variations, as in the concentration ranges ① and ② with $E_{a\mathrm{I}} \approx 87$ kJ/mol and $\tau_{o\mathrm{II}}^{-1} \approx 2 \times 10^{11}\ \mathrm{s}^{-1}$ for $x \approx 0.18$ [Fig. 12(a)]. A dramatic decrease of the activation energy and τ_o^{-1} parameter for the I_2 and I_3 branches [Figs. 12(a) and 12(b)] can be interpreted in terms of collective atomic displacements during these stages of the phase separation process. Therefore, one has to suppose that during the high-pressure synthesis large Si fcc clusters are formed in the Al-based solid solution. Thus, the relatively small $E_{a\mathrm{I}}$ and $\tau_{o\mathrm{I}}$ values observed for the I_2 and I_3 stages [Figs. 12(a) and 12(b)] can be attributed to the first stage of the phase separation process of the Si-cluster reconstruction and movement.

Finally, a strong lattice distortion and the formation of large nonequilibrium fcc Si clusters play possibly the key role for the appearance of the soft ''cluster phonon modes'' in substantially supersaturated solid solutions and for the enhancement of the electron-phonon interaction and the superconductivity in these materials.

V. CONCLUSIONS

The decay kinetics and nonequilibrium state parameters of supersaturated solid solutions $Al_{1-x}Si_x$ ($x<0.18$) have been studied comprehensively by resistivity relaxation and differential scanning calorimetry. It was shown that the decomposition process consists of two main stages I and II, where the first one includes the nucleation, growth, and coarsening stages usually observed for first-order phase transformations in metallic alloys. For the first stage, the activation energy $E_{a\mathrm{I}}\approx 80\pm 10$ kJ/mol can be attributed to the Si atom diffusion in the strongly distorted Al-based fcc matrix of the supersaturated solid solution produced under high pressure. Stage II follows to the nontraditional-type kinetics $\zeta\sim\exp[-(t/\tau)^{1/3}]$ both for isothermal relaxation and for the isochronal heat-release experimental results. The drastic increase of the heat-release contribution of the latest stage of the phase separation process (II) is observed for Si contents $x\approx 0.06-0.08$. Further elevation of the Si concentration in the fcc Al-based lattice causes the formation of fcc Si clusters during the high pressure synthesis procedure and initiates the splitting of the nucleation and growth process into three different branches. The analysis of the nonequilibrium state parameters during stage II allows one to suppose a transformation from fcc Si to tetrahedral Si inside large Si clusters embedded into the Al-rich matrix. The activation energy of this process $E_{a\mathrm{II}}\approx 130\pm 15$ kJ/mol can be attributed to the diffusion of Si atoms on large distances in a quite pure-Al matrix and can be understood in terms of the growing of the Si clusters up to a critical size.

ACKNOWLEDGMENTS

The authors are grateful to Dr. V. Yu. Ivanov and Dr. N. A. Samarin for experimental assistance and Professor S. V. Popova and Dr. A. G. Lyapin for helpful discussions. This work was supported by the INTAS program No. 96-451, Grants No. 17163 and No. 16067 of the Russian Foundation for Basic Research, Programs ''Fundamental Spectroscopy'' and ''Microwaves'' of the Russian Ministry of Science and Technology, Research Grant No. 96929 of the President of the Russian Federation, NATO Linkage Grants No. HTECH.LG.970342 and No. CN.SUPPL 973216, and Copernicus Network ERB IC15 CT98 0812. One of us (T.I.) wishes to thank the Humboldt Foundation for support.

*Present address: Institute of High Pressure Physics, Troitsk, 142092, Moscow District, Russia.

†Permanent address: General Physics Institute, Vavilov Str. 38, 117942, Moscow, Russia.

[1] H. Furukawa, Adv. Phys. **34**, 703 (1985).

[2] K. Binder, in *Materials Science and Technology*, edited by P. Haasen (VCH, Weinheim, 1991), Vol. 5, p. 405.

[3] J. D. Gunton, M. San-Miguel, and P. S. Sahni, in *Phase Transitions and Critical Phenomena*, edited by C. Domb and J. L. Lebowitz (Academic, New York, 1983), Vol. 8, p. 20.

[4] H. Mii, M. Senoo, and I. Fujishiro, Jpn. J. Appl. Phys. **15**, 777 (1976).

[5] V. F. Degtyareva, G. V. Chipenko, I. T. Belash, O. I. Barkalov, and E. G. Ponyatovskii, Phys. Status Solidi A **89**, K127 (1985).

[6] *Binary Alloy Phase Diagrams* edited by T. B. Massalski *et al.* (ASM International, Materials Park, OH, 1990), p. 212.

[7] N. E. Sluchanko, V. V. Glushkov, S. V. Demishev, N. A. Samarin, A. K. Savchenko, J. Singleton, W. Hayes, V. V. Brazhkin, A. A. Gippius, and A. I. Shulgin, Phys. Rev. B **51**, 1112 (1995).

[8] N. E. Sluchanko, V. V. Glushkov, S. V. Demishev, M. V. Kondrin, N. A. Samarin, A. K. Savchenko, A. O. Orlov, G. L. Snider, V. V. Brazhkin, and V. V. Moshchalkov, Phys. Rev. B **56**, 10 816 (1997).

[9] J. Chevrier, D. Pavuna, and F. Cyrot-Lackmann, Phys. Rev. B **36**, 9115 (1987).

[10] V. V. Brazhkin, A. G. Lyapin, S. V. Popova, and R. N. Voloshin, Phys. Status Solidi A **140**, 127 (1993).

[11] J. Chevrier, J. B. Suck, J. C. Lasjaunias, M. Perroux, and J. J. Capponi, Phys. Rev. B **49**, 961 (1994).

[12] L. G. Khvostancev, L. F. Vereschagin, and A. P. Novikov, High Temp.-High Press. **9**, 16 (1977).

[13] V. V. Brazhkin, V. V. Glushkov, S. V. Demishev, Yu. V. Kosichkin, N. E. Sluchanko, and A. I. Shulgin, J. Phys.: Condens. Matter **5**, 5933 (1993).

[14] H. Matyja, K. C. Russell, B. C. Giessen, and N. J. Grant, Metall. Trans. A **6**, 2249 (1975).

[15] P. van Mourik, E. J. Mittemeijer, and Th. H. de Keijser, J. Mater. Sci. **18**, 2706 (1983).

[16] C. Antonione, L. Battezzati, and F. Marino, J. Mater. Sci. Lett. **5**, 586 (1986).

[17] N. E. Sluchanko, V. V. Glushkov, S. V. Demishev, N. A. Samarin, A. K. Savchenko, and V. V. Brazhkin, J. Phys.: Condens. Matter **6**, 9079 (1994).

[18] V. V. Brazhkin, S. V. Popova, R. N. Voloshin, L. M. Stanev, and I. G. Spirov, High Press. Res. **6**, 333 (1992).

[19] J. W. Christian, *The Theory of Transformations in Metals and Alloys, Part I* (Pergamon, Oxford, 1975), p. 46.

[20] N. E. Sluchanko, V. V. Glushkov, S. V. Demishev, N. A. Samarin, and V. V. Brazhkin, Phys. Rev. B **53**, 11 304 (1996).

[21] J. R. Chelikowsky, Phys. Rev. Lett. **60**, 2669 (1988).

[22] J. R. Chelikovsky, K. M. Glassford, and J. C. Phyllips, Phys. Rev. B **44**, 1538 (1991).

[23] M. F. Jarrold and V. A. Constant, Phys. Rev. Lett. **67**, 2994 (1991).

[24] E. Kaxiras and K. Jackson, Phys. Rev. Lett. **71**, 727 (1993).

[25] U. Rothlishberger, W. Andreoni, and M. Parrinello, Phys. Rev. Lett. **72**, 665 (1994).

[26] O. Blaschko, P. Fratzl, G. Ernst, M. Bernole, and F. Fujara, Phys. Rev. B **30**, 6498 (1984).

[27] O. I. Barkalov, I. T. Belash, A. I. Kolesnikov, and Yu. M. Ostanevich, J. Non-Cryst. Solids **192-193**, 486 (1995).